HHS Public Access

Author manuscript

*J Nanosci Nanotechnol*. Author manuscript; available in PMC 2020 August 01.

Published in final edited form as:

*J Nanosci Nanotechnol*. 2019 August 01; 19(8): 4740–4746. doi:10.1166/jnn.2019.16348.

# Raman Signal Enhancement by Quasi-Fractal Geometries of Au Nanoparticles

**Richard E. Darienzo**, **Tatsiana Mironava**, **Rina Tannenbaum***

Biomedical Nanomaterials Research Laboratory, Department of Materials Science and Chemical Engineering, Stony Brook University, Stony Brook, NY 11794, USA

## Abstract

The synthesis of star-like gold nanoparticles (SGNs) in a temperature-controlled environment allows for temperature modulation and facilitates the growth of highly branched nanoparticles. By increasing the synthesis temperature, the level of branching increases as well. These highly branched features represent a distinctly novel, quasi-fractal nanoparticle morphology, referred to herein as gold nano caltrops (GNC). The increased surface roughness, local curvature and degree of inhomogeneity of GNC lend themselves to generating improved enhancement of the scattering signals in surface-enhanced Raman spectroscopy (SERS) via a mechanism in which the localized surface plasmon sites, or “hot spots,” provide the engine for the signal amplification, rather than the more conventional surface plasmon. Here, the synthesis procedure and the surface-enhancing capabilities of GNC are described and discussed.

### Keywords

Gold Nanoparticles; Surface-Enhanced Raman Scattering

## 1. INTRODUCTION

Raman spectroscopy is a non-destructive and sensitive technique that could be used, among a multitude of applications, for the exploration of the structure and chemical composition of biological materials.[1-5] It can constitute an effective tool for the delineation of cancer tissue, histological analysis of biopsies, *in vivo* detection of tumors and intraoperative imaging.[6-9] Raman spectroscopy is based on the inelastic scattering of monochromatic light upon interaction with molecular vibrations, phonons and other excitations, generating shifts in the energy of the incident light. The shift in energy gives information about the vibrational modes of the molecules in the system.[10, 11] Each molecule in a given system exhibits a precise set of vibrational modes, depending on their chemical composition, chemical environment and spatial organization. These vibrational modes constitute the fingerprints of the given system, and allow the identification of molecular species in the system and their interactions. Raman microscopy for biological and medical specimens generally uses near infrared (NIR) lasers (e.g., 785 nm laser), which reduces the risk of damaging the specimen by applying higher energy wavelengths and practically eliminates fluorescence.[12-19]

*Author to whom correspondence should be addressed.

In order to make the technique better suited for such biological applications, the surface-enhanced Raman scattering (SERS) technique, a variation of the original method, is particularly suitable.[20-24] This technique is based on the introduction of a rough metallic (e.g., Ag, Au or Cu) surface,[25-31] usually achieved by the presence of nanoparticles, which enhances the sensitivity of the measurement by at least $10^{10}$ and up to $10^{17}$ fold, depending on the type of nanoparticles, molecules probed, chemical and biological environment and incident light frequency.[32-35] The enhanced scattering effect is due to the excitation of the localized surface plasmons in the nanoparticles and the resulting interactions between the oscillations that are perpendicular to the surface and any molecules that are either physisorbed or chemisorbed on the surface. The closer the resonance of the incident light and the Raman signal are with the plasmon frequency, the higher the electric field amplification and the larger the enhancement.

In order to develop an imaging modality with a broad range of applications across various types of cancer tissues, the surface-enhancing nanoparticles must be chosen to provide a high level of signal resolution and scattering enhancement.[36-39] Gold nanospheres have shown to provide low and unstable enhancement levels, varying widely among individual particles and exhibiting susceptibility to environmental fluctuations.[40] Hence, the local fields associated with the excitation of surface plasmon resonances by the Raman source may not be the only mechanism responsible for the enhancement observed with metal nanoparticles. More recent explanations of the SERS effects by metal nanoparticles are based not only on intrinsic nanoparticle surface plasmons, but also on the presence of local field “hotspots”[41] due to surface roughness,[42] nanoscale voids between aggregated metallic nanoparticles,[43] or nanoscale gaps between nanoparticles and a metal surface.[44, 45] The SERS contribution of such hotspots can actually dominate the observed response.[46] An alternative way to increase the local electromagnetic field associated with the surface plasmon resonance would be to increase the local curvature of nanomaterials through the development of nanoscale surface inhomogeneities. For example, it was estimated that the vertices of silver nanotriangles exhibited 10 to 100 fold higher field strength compared to the surface of silver nanospheres of similar relative size.[47] Star-like gold nanoparticles (SGN), a new class of gold nanoparticle having sharp edges and tips, have been shown to exhibit a very high sensitivity to local changes in the dielectric environment, as well as larger enhancements of the electric field around the nanoparticles,[47] as compared with similar, less structurally-convoluted nanoparticles. Similar results have been found for other nanoparticles with sharp features.[39, 48, 49]

Based on these observations, our aim in this work was to develop various geometrical permutations of gold nanoparticles in addition to spheres and stars, and investigate their surface-enhancing Raman tural variations yielded a novel part prised of quasi-fractal branches, which we refer to as gold nano-caltrops (GNC). The underlying premise was that the extent of branching and the size of these nanoparticles would be closely correlated to their scattering ability. The gold nanoparticles were synthesized via the reduction of $HAuCl_4$ by hydroquinone.[38] The new quasi-fractal structure was achieved by varying the reaction temperature during synthesis. The first fractal branching features were observed at the reaction temperatures of 45 °C and became more pronounced as the reaction temperature was increased. Hence, we used the reaction temperature as a design parameter for the control

of the extent of fractal branching in gold nanocaltrops, and by association, in their expected Raman enhancement capabilities.

## 2. EXPERIMENTAL DETAILS

### 2.1. Nanoparticle Synthesis

All chemicals for the nanoparticle synthesis were purchased from Sigma Aldrich (St. Louis, MO). De-ionized water was obtained from a Millipore (Billerica, MA) Direct Q3 water filtration system. The synthesis was carried out in a three-neck flask fitted with a 400 mm Graham type condenser to create a reflux system. The flask was filled with 10 mL of deionized water at room temperature with a magnetic stirrer set to 500 rpm, and was held in a water bath. Nine $\mu$L of an $HAuCl_4$ solution with a 1:10 dilution and containing 17 wt.% Au was added to the water in the flask and mixed for several minutes to allow the temperature of the gold solution to equilibrate with that of the bath. Next, 100 $\mu$L of 11 mg/mL hydroquinone, $C_6H_4(OH)_2$, was injected into the solution.[38, 49, 50] Within minutes, the reaction mixture changed in color from pale yellow to light blue. After 5 minutes of mixing, 20 $\mu$L of 10 mg/mL sodium citrate tribasic dehydrate, $Na_3C_6H_5O_7 \cdot 2H_2O$, was added to function as a capping agent for the growing particles. The addition of the sodium citrate was also shown to increase the long-term stability of the nanoparticles while in solution.[38]

The reaction conditions were controlled by changing the temperature of the water bath. The particles synthesized at 65 ° were placed in a water bath and held at approximately 8 °C for 15 minutes before being allowed to reach room temperature.

### 2.2. Characterization Techniques

**2.2.1. UV-Vis Spectroscopy—**The absorption profiles of the nanoparticle suspensions were analyzed with a Thermo Fisher Scientific Evolution 220 Ultraviolet-Visible Spectrometer (UV-Vis). Nanoparticle suspensions were first stirred vigorously before aliquots were deposited into a quartz cuvette (VWR, Radnor, PA). Spectra were obtained over the range of 190–1100 nm at

**2.2.2 Electron Microscopy—**A 5 $\mu$L aliquot of a nanoparticle sample was deposited on a copper grid (Ted Pella, Formvar/carbon 400 mesh, Redding, CA) and allowed to dry overnight. The grids were used for both transmission and scanning electron microscopy imaging experiments.

Transmission electron microscopy (TEM) and scanning electron microscopy (SEM) experiments were performed on a JEOL JEM-1400 electron microscope at 120.0 kV and JEOL JSM-7600F field emission SEM at 5.0 kV, respectively.

**2.2.3. Particle Size Analysis—**Dynamic light scattering (DLS) measurements were performed on a Malvern Zetasizer (Nano-ZS) at 25.0 °C with the refractive index and absorption set to 1.400 and 0.100, respectively. TEM micrographs were used to evaluate particle size as well. The average nanoparticle sizes were evaluated by calculating the log

mean average of the core and outer spike radii of each nanoparticle, followed by number-averaging over the entire nanoparticle population on the micrographs used.

**2.2.4. Raman Spectroscopy—**Substrates for surface enhanced Raman Spectroscopy (SERS) experiments were prepared using pre-cut *p*-type (boron) silicon wafers (Ted Pella, 5 × 5 mm diced). Silicon sections were thoroughly washed in a 1:100 (v/v) solution of 37% HCl (Fisher Scientific) with 70% ethanol (Fisher Scientific). The sections were then rinsed with copious amounts of deionized water and allowed to dry. The clean and dry silicon sections were next placed in a 0.01% (w/v) poly-L-lysine solution (Sigma Aldrich) for 5 minutes. After that, the silicon sections were placed in a 60 °C oven for 1 hour to dry. The silicon sections were then submerged in nanoparticle suspensions and allowed to incubate for 24 hours at room temperature before being removed and allowed to dry. Fifteen $\mu$L aliquots of $5.2 \cdot 10^{-4}$ mg/mL malachite green (MG) dye (Sigma Aldrich) solution was then applied to the samples by drop casting. SERS measurements were performed on a HORIBA XploRA PLUS Raman microscope with a Marhauzer motorized stage. Spectra were collected utilizing a 638 nm laser at 1% laser power, 600 gr/mm grating, 100 $\mu$m hole, 50 $\mu$m slit, and with a 0.5 sec acquisition time with 1 acquisition per step and 100× objective. Data for each sample was obtained from three maps measuring 80 × 80 $\mu m^2$ with a step size of 0.2 $\mu$m that was chosen at random. A contour area of 5 $\mu m^2$ was placed at the location where the highest intensity Raman signal was detected, and all the spectra contained therein were averaged. This process was repeated for each of the three maps generated from each sample and then averaged together in order to better portray the average Raman enhancement provided by each sample.[38] Collected spectra were then processed identically to remove fluorescence and cosmic rays by first extracting the data over the range of 150–2000 $cm^{-1}$, followed by the subtraction of a 9th degree polynomial background from each spectrum.

**2.2.5. Perimetric Ratio Evaluation—**Perimetric ratio analysis: The Matlab code for the evaluation of the perimetric ratio is listed below:

I = imread(‘rina.png’); Load image

level = graythresh(I); Find the threshold for image

BW = imbinarize(I,level); Turn image into binary

WB = imcomplement(BW); reverse black and white

(to use Matlab functions)

AR = bwarea(WB); area of white region

PP = regionprops(WB,‘Perimeter’); list of lengths of all

white regions

Big = largest of PP.Perimeter; this will give length of largest white region

BIG^2/AR = isoperimetric ratio ≥ 4 pi (the larger it is, the more fractal the shape).

## 3. RESULTS AND DISCUSSION

### 3.1. Particle Size and Geometry

SERS activity is correlated to the size, shape and geometry of nanoparticles,[50, 51] and hence, controlling these parameters is essential in producing SERS probes with consistent enhancement behavior, as well as enabling the appropriate choice of excitation laser to engage the surface plasmon and the local surface plasmon resonance (LSPR) effects.

Star-like gold nanoparticles (SGN) were obtained at 25 °C,[38, 51] and gold nano-caltrops (GNC) consisting of quasi-fractal particles, were obtained at 65 °C, as illustrated in the TEM images shown in Figures 1(a), (b), respectively, and the SEM image shown in Figures 1(c), (d), respectively. As can be seen from the images of the Au nanoparticle at these two temperatures, the overall size of the SGN is smaller than that of the GNC, however the GNC have a higher degree of surface inhomogeneity. The average sizes of the nanoparticles based on the TEM images were calculated by using the log mean average of the core and outer radii of each nanoparticle, shown in Figure 2(a) for the SGNs and Figure 2(b) for the GNCs. This procedure is described by:

$$R_{\mathrm{LM}} = \frac{R_{\mathrm{Spike}} - R_{\mathrm{Core}}}{\ln(R_{\mathrm{Spike}} / R_{\mathrm{Core}})} \quad (1)$$

where $R_{\mathrm{Core}}$ is the average radius of the inner solid sphere at the center of the nanoparticles and is encased by the inner circle, as shown in Figure 2(a), and $R_{\mathrm{Spike}}$ is half of the average distance between two branches at opposite sides of the nanoparticles that are encased in the outer circle, as shown in Figure 2(b).

Based on TEM images, the average radius-equivalent size of SGNs was 43 ± 22 nm and of GNCs was 168 ± 60 nm. The particle size values obtained from TEM images were then compared to the values obtained from DLS measurements, as shown in Figure 2(c). Based on the DLS measurements, the average radius-equivalent size of SGNs was 79 ± 48 nm and of GNCs was 179 ± 55 nm. The slightly larger values from DLS measurements are not surprising since DLS estimates size distribution differently, i.e., by size to the power of six, and therefore, larger particles are given more weight. Moreover, DLS measures the hydrodynamic radii of particles that includes adsorbed species and solvent interactions, while in the TEM image only the metallic moiety is observed due to the insufficient contrast of other organic moieties. A rough quantitative estimate of the degree of surface roughness and branching was calculated by the evaluation of the isoperimetric ratio, $P = L^2/A$, where $L$ is the length of the closed loop curve encompassing the nanoparticle and $A$ is the area enclosed in the closed loop curve (see Matlab code in the Experimental Details section). The calculated values of $P$ for the gold nanoparticles were 24.1 and 34.4 for the SGNs and GNCs, respectively, as shown in Figure 2(d). The departure from the value of $4\pi$ (for a perfect circle) is indicative of the extent of deviation of the curve from a circular shape, and hence, a good measure of the degree of fractal character.

Previous studies have shown that the growth dynamics of branched particles having higher energy surfaces was the result of kinetically-favored growth regimes.[39, 58-60] This type of growth process was shown to be driven by the relatively low reduction potential of hydroquinone, which acts as a reducing agent in this process.[60-63] We therefore assume that increasing the synthesis temperature increases the reaction kinetics, which in turn, augments the effect of the hydroquinone on the already rapid deposition process of $Au^0$ onto the (111) planes of the gold. As has been previously demonstrated,[39, 51] a higher deposition rate of $Au^0$ is key to the formation of branch structures on nanoparticles, such as star-like particles and in our case, quasi-fractal structures.

### 3.2. Surface Plasmon Resonance

When the synthesis temperature was increased from 25 °C to 65 °C, the resulting UV-Vis spectra exhibited a drastic reduction in intensity and detail, as shown in Figure 3. At 25 °C, the spectrum exhibits two major peaks in the 500–800 nm region of interest (see inset of Fig. 3). The peak at 531 nm is consistent with the surface plasmon resonance observed for spherical gold nanoparticles in the approximate 20–60 nm size range, which is the overall average size diameter of the particles obtained at the lower temperature. However, the particles have a star-like structure, and hence their spectra are more complex, as evidences by the presence of a second peak at 624 nm.[64-70] The presence of this peak and the overall broadening of the spectrum, as compared to that of spherical gold nanoparticles of similar size, is mostly due to two distinct phenomena: (a) The departure from the spherical geometry and the breakdown in particle symmetry give rise to multiple axes of varying size and varying geometries, and as a result, exhibit distinct surface plasmons. Previous characterization of gold nanorods highlighted the fact that these nanoparticles possess two absorption peaks,[64, 65] one that originates because of plasmons on the transverse axis that coincides with the absorption of a spherical particle of similar size, and another that originates from the longitudinal axis and is considerably red-shifted. Similarly, the presence of these types of anisotropic features in the star-like gold nanoparticles contribute to the emergence of the double peak that we observe in our system, (b) Another feature of the star-like gold nanoparticles is a broad size distribution, which causes both the presence of the second peak at lower frequencies and an overall broadening of the peaks in the spectrum.

The broadening and the decreasing intensity of the absorption peaks for the gold quasi-fractal gold nanoparticles obtained at 65 °C is believed to be the result of two major factors, i.e., the addition of more fractal features as well as the increasing particle size. The fractal contribution is due to the presence of multiple axes of varying sizes,[66] thus most likely causing multiple absorption peaks of low intensity that merge into one broad unresolved absorption band. The multiplicity in branch morphologies and dimensions prevents any dominant shape feature from being expressed on all of the nanoparticles, and hence, no specific $\lambda_{max}$, i.e., wavelength at which maximum absorption occurs, is observed. The absorption spectrum of a ten-fold concentrated solution of the quasi-fractal nanoparticles exhibited similar broad and flat features, indicating that these characteristics are concentration independent.

### 3.3. Enhancement of Raman Scattering

The increase in the expected SERS enhancement with increasing nanoparticle size has traditionally been attributed to the larger surface area associated with larger particles.[52-54] However, the SERS enhancement does not depend solely on the surface area of the nanoparticles but also on the enhanced electromagnetic field generated from the surface plasmon. While increase in particle size increases the local electromagnetic enhancement,[55] it also generates a decrease in surface curvature, absorption of the incident light and inelastic scattering that occur on the surface. These phenomena actually lead to a weakening of the electromagnetic field on the surface and a decrease in the overall SERS intensity.[56] Hence, size alone would not be the best or the most reliable predictor as to the efficiency of the SERS enhancement.

Another possible predictor of SERS enhancement would be the magnitude of the surface plasmon, as indicated by the absorption spectra of the nanoparticles.[68, 71, 72] However, as we have previously shown, the intensity of the absorption spectra is strongly impacted not only by the size of the particles, but more importantly, by the roughness of the surface and the local curvature of the characteristic geometrical constituents of the nanostructures. Again, what we observed and showed in Figure 3, was that nanoparticles having a quasi-fractal surface morphology, exhibited an almost complete absence of a discernable absorption spectrum.

The enhancement of the Raman spectrum of a triarylmethane dye with the general formula $\{C_6H_5C\ [C_6H_4N(CH_3)_2]_2\}(C_2O_3OH)$ (malachite green oxalate salt, MG) when incubated with either gold nanostars or gold quasi-fractal nanoparticles is shown in Figure 4. All Raman spectra were obtained under identical settings in order to enable quantitative comparisons between all of the samples. The most important consideration was the establishment of the optical plane where the laser was focused in order to provide the common conditions for all the samples. The plane of focus determines the interaction volume of the laser in the sample and can easily be tuned within the thin films created by the poly-L-lysine or dye. This may cause inconsistent interaction volumes and artificially affect the maximum signal obtained in units of counts/sec. In order to circumvent this, each sample was first positioned so that an area devoid of sample could be probed by the laser. The laser was then focused using an auto-focusing routine that sought to maximize the Raman signal of the Si spectral line at 520 $cm^{-1}$ by adjusting the height of the sample. Once this height was established, samples were mapped with all room lights turned off. Any further inconsistencies between samples was then limited to the distributions of particles and dye on the poly-L-lysine coated Si substrates.

As shown in Figure 4, the enhancement of the Raman scattering spectrum of MG due to the presence of the quasi-fractal nanoparticles is quite remarkable. Since the main interest in this work was to probe the effect of geometrical permutations of gold nanoparticles on their surface-enhancing Raman capabilities, we found it particularly revealing to calculate the relative enhancement factor of the quasi-fractal nanoparticles as compared to the star-like nanoparticles.[30, 73]

The enhancement factor (*EF*) is given by:

$$EF = \frac{N_{\mathrm{Vol}} \cdot I_{\mathrm{Surf}}}{N_{\mathrm{Surf}} \cdot I_{\mathrm{Vol}}} \tag{2}$$

where $N_{\mathrm{Vol}}$ and $N_{\mathrm{Surf}}$ are the number of analyte molecules in the probed liquid sample and on the SERS substrates, respectively, and $I_{\mathrm{Vol}}$ $I_{\mathrm{Surf}}$ are the corresponding intensities of the normal Raman and the SERS spectra.

The relative level of enhancement provided by the GNCs in comparison to the SGNs is given by:

$$\begin{aligned} EF_{\mathrm{rel}} = \frac{EF_{\mathrm{GNC}}}{EF_{\mathrm{SGN}}} &= \frac{(N_{\mathrm{Vol}} \cdot I_{\mathrm{Surf}} \,/\, (N_{\mathrm{Surf}} \cdot I_{\mathrm{Vol}}))_{\mathrm{GNC}}}{(N_{\mathrm{Vol}} \cdot I_{\mathrm{Surf}} \,/\, (N_{\mathrm{Surf}} \cdot I_{\mathrm{Vol}}))_{\mathrm{SGN}}} \\ &= \frac{I_{\mathrm{Surf}}^{\mathrm{GNC}}}{I_{\mathrm{Surf}}^{\mathrm{SGN}}} \cdot \frac{N_{\mathrm{Surf}}^{\mathrm{SGN}}}{N_{\mathrm{Surf}}^{\mathrm{GNC}}} \end{aligned} \tag{3}$$

The assumption is that the number of analyte molecules in the probed liquid sample is independent of the nanoparticles used to generate the signal enhancement and hence, the quantity $N_{\mathrm{Vol}}/I_{\mathrm{Vol}}$ in both systems is constant. If we assume that the densities of the analyte molecules on or in the proximity of the surface of the gold nanoparticles is similar for both nanoparticle geometries, then $N_{\mathrm{Surf}}^{\mathrm{SGN}} \,/\, N_{\mathrm{Surf}}^{\mathrm{GNC}} \propto P^{\mathrm{GNC}} \,/\, P^{\mathrm{SGN}}$, where $P^{\mathrm{GNC}}$ is the isoperimetric ratio for the quasi-fractal gold nanoparticles and $P^{\mathrm{SGN}}$ is the isoperimetric ratio for the star-like gold nanoparticles. Therefore, the relative ratio becomes:

$$EF_{\mathrm{rel}} = \frac{I_{\mathrm{Surf}}^{\mathrm{GNC}}}{I_{\mathrm{Surf}}^{\mathrm{SGN}}} \cdot \frac{P^{\mathrm{GNC}}}{P^{\mathrm{SGN}}} \tag{4}$$

The three main characteristic and most prominent Raman bands of MG are observed at 1612 $\mathrm{cm}^{-1}$, 1377 $\mathrm{cm}^{-1}$ and 1172 $\mathrm{cm}^{-1}$, corresponding to symmetric ring breathing and C–C stretching of the aromatic rings, the phenyl-N stretch and the symmetric in-plane and out-of-plane bending of the rings, respectively.[74, 75] The intensity of the 1172 $\mathrm{cm}^{-1}$ Raman shift band of MG was 98 counts/s in the presence of SGNs ($I_{\mathrm{Surf}}^{\mathrm{SGN}}$), and 1755 counts/s in the presence of GNCs ($I_{\mathrm{Surf}}^{\mathrm{GNC}}$). Based on these values, the calculated relative enhancement ratio $EF_{\mathrm{rel}}$ is 29.2. It is interesting to note that the relative enhancement ratio is not the same for all frequencies, fact which may be indicative of some preferential orientation of the MG molecules near or at the surface of the gold nanoparticles.

The considerable greater enhancement of the Raman signals in the presence of the quasi-fractal gold nanoparticle as compared to that obtained in the presence of star-like gold nanoparticles, demonstrates that the mechanism of enhancement is not dependent primarily on the magnitude of the surface plasmon resonance of the nanoparticles, as traditionally believed. Instead, the enhancement is due to local “hot spots”[41-46, 66] and therefore, highly

dependent on the inhomogeneity of the surface features, i.e., both the surface roughness, degree of branching and variations in local surface curvature.

## 4. CONCLUSIONS

In this work, we described a procedure for synthesizing gold nanoparticles having a novel, quasi-fractal morphology, which we termed gold nano-caltrops (GNC). This highly branched nanoparticle morphology is the result of the temperature modulation to the conventional one-pot synthesis of star-like gold nanoparticles. These GNC possess a high degree of surface roughness thanks to the kinetics favored growth regime facilitated through a combination of the presence of hydroquinone as the reducing agent and higher synthesis temperatures. As a result of their highly-curved, sharp and irregular surface features, these nanoparticles exhibited marked enhancement of Raman signals of a reporter dye when compared with similar nanoparticles that possess less overall surface roughness, such as star-like nanoparticles. Moreover, we have shown that the mechanism of enhancement of the Raman signals by these quasi-fractal nanoparticles was not necessarily correlated to their surface plasmon resonance, but rather to the degree of their surface inhomogeneity. Hence, such highly branched nanoparticles might provide higher resolution and higher sensitivity for the detection of low concentration analyte molecules.

## Acknowledgments:

The authors thank Dr. Fran Adar from Horiba for her guidance with Raman spectroscopy, Professor Ming-Yu Ngai and Johnny Lee from the Department of Chemistry at Stony Brook University, and undergraduate students Olivia Chen and Maurinne Sullivan for their technical assistance. The authors also thank Professor Allen Tannenbaum from the Departments of Computer Sciences and Applied Mathematics at Stony Brook University for providing the Matlab code for the calculation of the isoperimetric ratios. This research was partially funded through the Stony Brook Scholars in Biomedical Sciences Program. This research used resources of the Center for Functional Nanomaterials, which is a U.S. DOE Office of Science Facility at the Brookhaven National Laboratory under Contract No. DE-SC0012704.

## References and Notes

1. Seklar Talari AC, Movasaghi Z, Rehman S, and Ur Rehman I, Appl. Spec. Rev 50, 46 (2015).
2. Hanlon EB, Manoharan R, Koo T-W, Shafer KE, Motz JT, Fitzmaurice M, Kramer JR, Itzkan I, Dasari RR, and Feld MS, Phys. Med. Biol 45, R1 (2000). [PubMed: 10701500]
3. Petryayeva E and Krull U, Anal. Chim. Acta 706, 8 (2011). [PubMed: 21995909]
4. Schlücker S, Angew. Chem. Int. Ed 53, 4756 (2014).
5. Jain PK, Huang X, El-Sayed IH, and El-Sayed MA, Plasmonics 2, 107 (2007).
6. Vendrell M, Maiti K, Dhaliwal KK, and Chang YT, Trends Biotechnol. 31, 249 (2013). [PubMed: 23416096]
7. Zhang Y, Hong H, and Cai W, Curr. Pharm. Biotechnol 11, 654 (2010). [PubMed: 20497112]
8. Jokerst JV and Gambhir SS, Acc. Chem. Res 44, 1050 (2011). [PubMed: 21919457]
9. Yang J, Wang Z, Zong S, Song C, Zhang R, and Cui Y, Anal. Bioanal. Chem 402, 1093 (2012). [PubMed: 22124755]
10. Fan M, Andrade GFS, and Brolo AG, Anal. Chim. Acta 693, 7 (2011). [PubMed: 21504806]
11. Smith ZJ and Berger AJ, Opt. Lett 3, 714 (2008).
12. Urabe H, Tominaga Y, and Kubota K, J. Chem. Phys 78, 5937 (1983).
13. Chou KC, Biochem. J 215, 465 (1983). [PubMed: 6362659]
14. Chou KC, Biochem. J 221, 27 (1984). [PubMed: 6466317]

15. Urabe H, Sugawara Y, Ataka M, and Rupprecht A, Biophys. J 74, 1533 (1988).
16. Chou KC, Biophys. Chem 30, 3 (1988). [PubMed: 3046672]
17. Chou KC, Trends. Biochem. Sci 14, 212 (1989). [PubMed: 2763333]
18. Schütz M, Müller CI, Salehi M, Lambert C, and Schlücker S, J. Biophoton 4, 453 (2011).
19. Ellis D and Goodacre R, Analyst 131, 875 (2006). [PubMed: 17028718]
20. Qian X, Peng X, Ansari DO, Yin-Goen Q, Chen GZ, Shin DM, Yang L, Young AN, Wang MD, and Nie S, Nature Biotech. 26, 83 (2008).
21. Michalet X, Pinaud FF, Bentolila LA, Tsay JM, Doose S, Li JJ, Sundaresan G, Wu AM, Gambhir SS, and Weiss S, Science 307, 538 (2005). [PubMed: 15681376]
22. Lee S, Kim S, Choo J, Shin SY, Lee YH, Choi HY, Ha S, Kang K, and Oh CH, Anal. Chem 79, 916 (2007). [PubMed: 17263316]
23. Jokerst JV, Miao Z, Zavaleta C, Cheng Z, and Gambhir SS, Small 7, 625 (2011). [PubMed: 21302357]
24. Gregas MK, Yan F, Scaffidi J, Wang HN, and Vo-Dinh T, Nanomed. Nanotech. Biol. Med 7, 115 (2011).
25. Moskovits M, Topics in Applied Physics, edited by Kneipp K, Moskovits M, and Kneipp H, Springer, Berlin, Heidelberg (2006), Vol. 103, pp. 1–17.
26. Campion A and Kambhampati P, Chem. Soc. Rev 27, 241 (1998).
27. Creighton JA and Eadon DG, J. Chem. Soc. Faraday Trans 87, 3881 (1991).
28. Langhammer C, Yuan Z, Zorić I, and Kasemo B, Nano Lett. 6, 833 (2006). [PubMed: 16608293]
29. Blackie EJ, Le Ru EC, and Etchegoin PG, J. Amer. Chem. Soc 131, 14466 (2009). [PubMed: 19807188]
30. Le Ru EC, Blackie E, Meyer M, and Etchegoin PG, J. Phys. Chem. C 111, 13794 (2007).
31. Lal S, Link S, and Halas NJ, Nature Photon. 1, 641 (2007).
32. Lu H, Zhang H, Yu X, Zeng S, Yong KT, and Ho HP, Plasmonics 7, 167 (2011).
33. Bao LL, Mahurin SM, Liang CD, and Dai S, J. Raman Spectr 34, 394 (2003).
34. Ayas S, Cinar G, Ozkan AD, Soran Z, Ekiz O, Kocaay D, Tomak A, Toren P, Kaya Y, Tunc I, Zareie H, Tekinay T, Tekinay AB, Guler MO, and Dana A, Sci. Rep 3, 2624 (2013). [PubMed: 24022059]
35. Cao YC, Jin R, and Mirkin CA, Science 297, 1536 (2002). [PubMed: 12202825]
36. Haynes CL, McFarland AD, and Van Duyne RP, Anal. Chem 77, 338A (2005).
37. Liao PF and Wokaun A, J. Chem. Phys 76, 751 (1982).
38. Morasso C, Mehn D, Vanna R, Bedoni M, Forvi E, Colombo M, Prosperi D, and Gramatica F, Mater. Chem. Phys 143, 1215 (2014).
39. Bakr OM, Wunsch BH, and Stellacci F, Chem. Mater 18, 3297 (2006).
40. Wustholz KL, Henry AI, McMahon JM, Freeman RG, Valley N, Piotti ME, Natan MJ, Schatz GC, and Van Duyne RP, J. Am. Chem. Soc 132, 10903 (2010). [PubMed: 20681724]
41. Moskovits M, Phys. Chem. Chem. Phys 15, 5301 (2013). [PubMed: 23303267]
42. Kneipp K, Kneipp H, Itzkan I, Dasari RR, and Feld MS, J. Phys. Condens. Matter 14, R597 (2002).
43. Aravind PK, Rendell RW, and Metiu H, Chem. Phys. Lett 85, 396 (1982).
44. Aravind PK and Metiu H, Surf. Sci 124, 506 (1983).
45. Fang Y, Seong NH, and Dlott DD, Science 321, 388 (2008). [PubMed: 18583578]
46. Tiwari VS, Oleg T, Darbha GK, Hardy W, Singh JP, and Ray PC, Chem. Phys. Lett 446, 77 (2007).
47. Hao F, Nehl CL, Hafner JH, and Nordlander P, Nano Lett. 7, 729 (2007). [PubMed: 17279802]
48. Nehl CL, Liao H, and Hafner JH, Nano Lett. 6, 683 (2006). [PubMed: 16608264]
49. Tian F, Bonnier F, Casey A, Shanahan AE, and Byrne HJ, Anal. Methods 6, 9116 (2014).
50. Link S and El-Sayed MA, J. Phys. Chem. B 103, 4212 (1999).
51. Li M, Cushing SK, Zhang J, Lankford J, Aguilar ZP, Ma D, and Wu N, Nanotechnol. 23, 115501 (2012).
52. Hong S and Li X, J. Nanomater 2013, 790323 (2013).

53. Lin KQ, Yi J, Hu S, Liu BJ, Liu JY, Wang X, and Ren B, J. Phys. Chem. C 120, 20806 (2016).
54. Quester K, Avalos-Borja M, Vilchis-Nestor AR, Camacho-López MA, and Castro-Longoria E, PLOS One 8, e77486 (2013). [PubMed: 24130891]
55. Kelly KL, Coronado E, Zhao LL, and Schatz GC, J. Phys. Chem. B 107, 668 (2003).
56. Stiles PL, Dieringer JA, Shah NC, and Van Duyne RP, Annu. Rev. Anal. Chem 1, 601 (2008).
57. Driskell JD, Lipert RJ, and Porter MD, J. Phys. Chem. B 110, 17444 (2006). [PubMed: 16942083]
58. Perrault SD and Chan WCW, J. Am. Chem. Soc 131, 17042 (2009). [PubMed: 19891442]
59. Langille MR, Personick ML, Zhang J, and Mirkin CA, J. Am. Chem. Soc 134, 14542 2).
60. Sirajuddin U, Mechlerc A, Torriero AAJ, Nafady A, Lee CY, Bond AM, O'Mullane AP, and Bhargava SK, Coll. Surf. A 370, 35 (2010).
61. Morasso C, Picciolini S, Schiumarini D, Mehn D, Ojea-Jiménez I, Zanchetta G, Vanna R, Bedoni M, Prosperi D, and Gramatica F, J. Nanopart. Res 17, 330 (2015).
62. Li J, Wu J, Zhang X, Liu Y, Zhou D, Sun H, Zhang H, and Yang B, J. Phys. Chem. C 115, 3630 (2011).
63. Zhang X, Tang K, Yang Q, Qi L, Wang X, Chen F, and Chen Z, Mater. Lett 140, 180 (2015).
64. Link S and El-Sayed MA, J. Phys. Chem. B 103, 8410 (1999).
65. Ghosh SK and Pal T, Chem. Rev 107, 4797 (2007). [PubMed: 17999554]
66. Willets KA and Van Duyne RP, Annu. Rev. Phys. Chem 58, 267 (2007). [PubMed: 17067281]
67. Haiss W, Thanh NTK, Aveyard J, and Fernig DG, Anal. Chem 79, 4215 (2007). [PubMed: 17458937]
68. Daniel MC and Astruc D, Chem. Rev 104, 293 (2004). [PubMed: 14719978]
69. Grzelczak M, Juste JP, Mulvaney P, and Marzán LML, Chem. Soc. Rev 37, 1783 (2008). [PubMed: 18762828]
70. El-Brolossy TA, Abdallah T, Mohamed MB, Abdallah S, Easawi K, Negm S, and Talaat H, Eur. Phys. J. Spec. Topics 153, 361 (2008).
71. Cheng JX and Xie XS, J. Phys. Chem. B 108, 827 (2004).
72. Zeng S, Yong K-T, Roy I, Dinh X-Q, Yu X, and Luan F, Plasmonics 6, 491 (2011).
73. McFarland AD, Young MA, Dieringer JA, and Van Duyne RP, J. Phys. Chem. B 109, 11279 (2005). [PubMed: 16852377]
74. Pettinger B, Ren B, Picardi G, Schuster R, and Ertl G, J. Raman Spectr 36, 541 (2005).
75. Zhang Y, Huang Y, Zhai F, and Lai K, Food Chem. 135, 845 (2005).

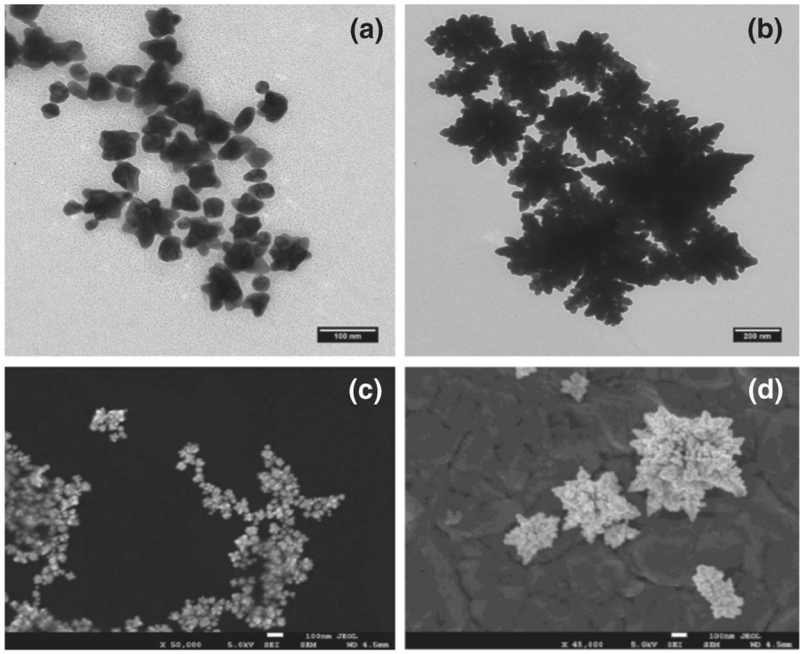


**Figure 1.**

Morphology of the synthesized nanoparticles showing the details of surface features. (a) Transmission electron micrograph of star-like gold nanoparticles (SGN) at a magnification of 125,000; (b) Transmission electron micrograph of quasi-fractal gold nanoparticles (GNC) at a magnification of 125,000; (c) Scanning electron micrograph of star-like gold nanoparticles; (d) Scanning electron micrograph of quasi-fractal gold nanoparticles.

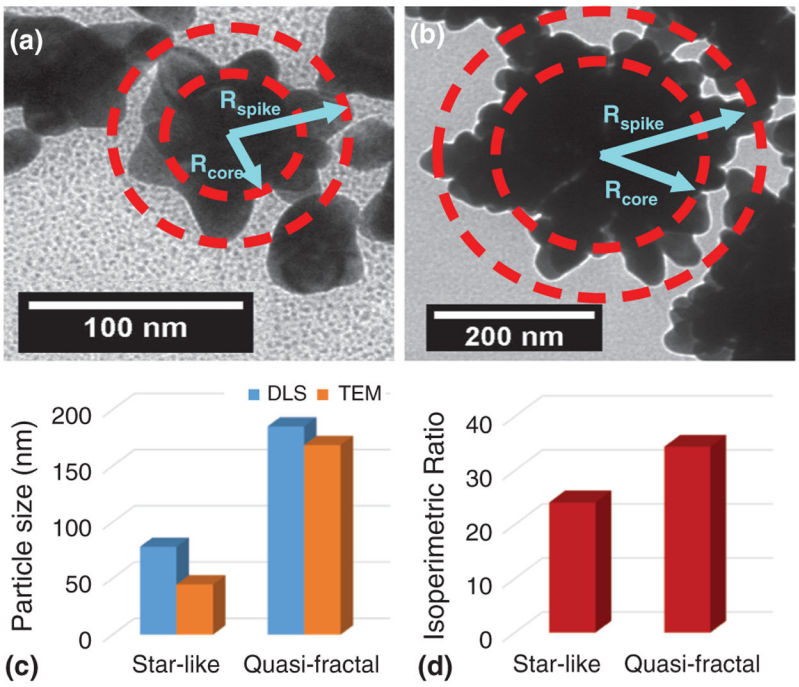


**Figure 2.**

Evaluation of particle size and particle morphology. (a) Schematic description for the calculation of the log mean radius of star-like gold nanoparticles; (b) Schematic description for the calculation of the log mean radius of quasi-fractal gold nanoparticles. The log mean radius-equivalent for both types of nanoparticles was calculated using the log mean equation where the core radius was the distance from the center of the particle to the edge of the solid inner core and the outer radius was half the distance between two spikes on opposite sides of the nanoparticles. The overall equation used is given by: $R_{LM} = (R_{Spike} - R_{Core})/\ln(R_{Spike}/R_{Core})$; (c) Comparison of particles sizes obtained from transmission electron micrographs and from dynamic light scattering experiments; (d) The isoperimetric ratios for both star-like and quasi-fractal gold nanoparticles calculated using Matlab.

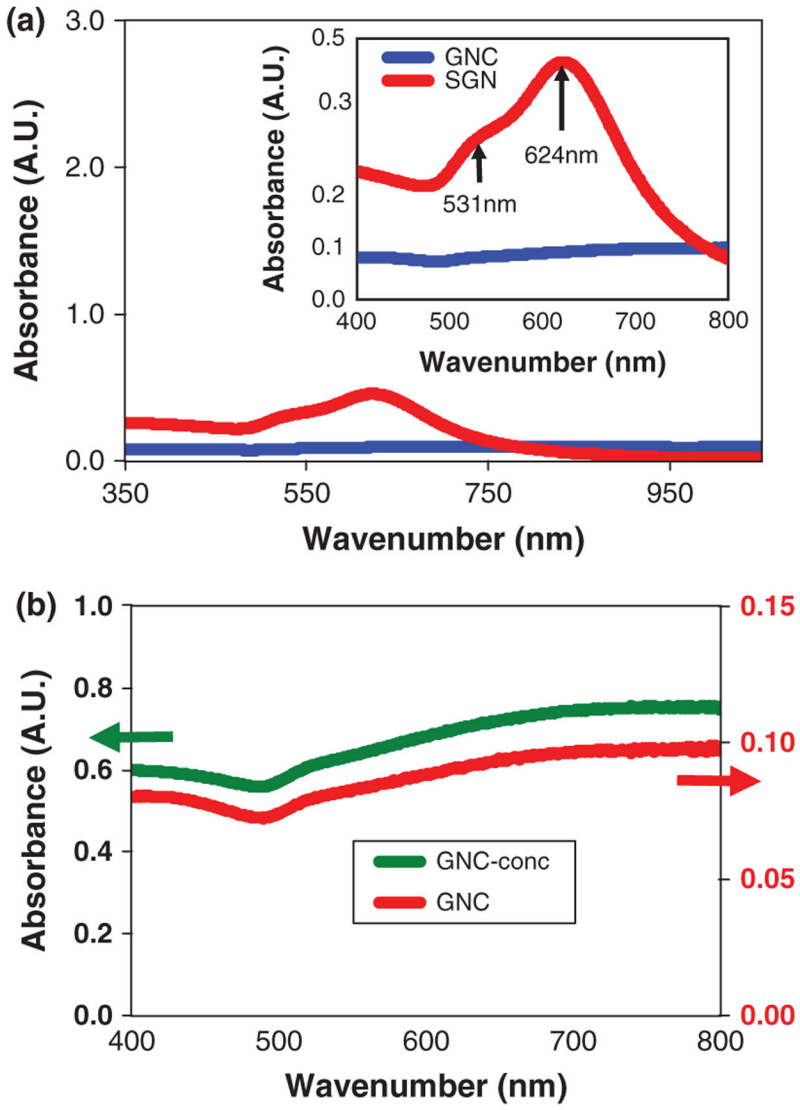


**Figure 3.**

The UV-Vis absorption spectrum for both star-like and quasi-fractal gold nanoparticles. (a) The drastic reduction in spectral intensity and detail with the increase of synthesis temperature from 25 °C to 65 °C. At 25 °C, the spectrum exhibits two major peaks in the 500–800 nm region of interest (inset). (b) The comparison of the absorption spectra of an as-prepared suspension of quasi-fractal nanoparticles at 65 °C with a ten-fold concentrated suspension at the same temperature.

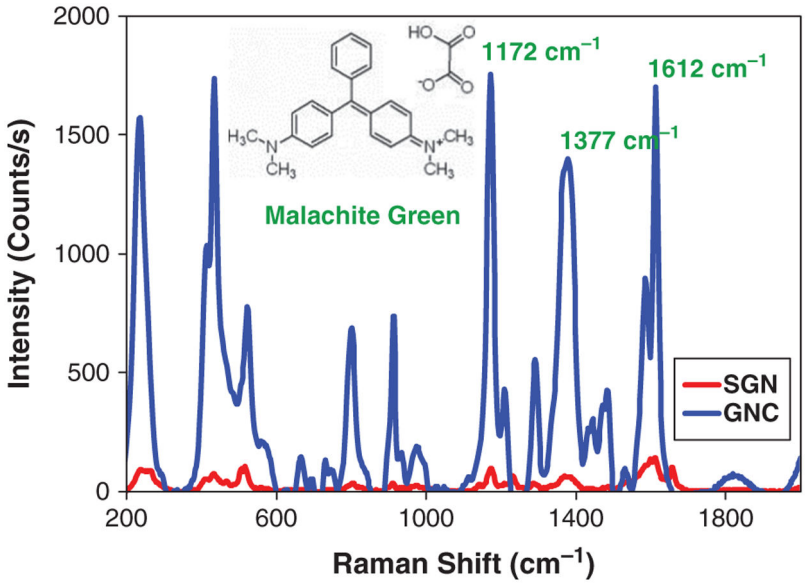


**Figure 4.**

Comparison of the Raman spectra of malachite green dye in the presence of star-like and quasi-fractal gold nanoparticles. The chemical structure for the malachite green oxalate salt molecule is also shown, together with the three most noteworthy characteristic Raman bands of the dye. The intensity of the 1172 $cm^{-1}$ band was used as the basis for the calculation of the relative enhancement factor.